Chapter 3 Manganese Oxide-Carbon Nanotube Nanocomposite Supercapacitor Electrodes

3.1 Structural analysis of MnO_x/Ni and MnO_x/CNTs/Ni composite electrodes

The FE–SEM image of the CNTs/Ni substrate is shown in Fig. 3.1, indicating that the CNTs electrophoretically deposited on the Ni substrate have the diameters range between 20 and 30 nm. These CNTs are randomly distributed, entangled and cross linked on the Ni substrate. The surface of the electrode becomes rough after CNT deposition. The evidence for this has been derived from the BET surface area measurements of the Ni and CNTs/Ni substrates, which are calculated as 0.7 and 14.9 m^2/g, respectively. The BET surface area increases with the deposition of the high–surface–area CNTs (~298.7 m^2/g based on the mass of CNTs only) on the Ni substrate.

Then, the $MnO_x \cdot nH_2O$ films were anodic deposited on the Ni and CNTs/Ni substrates. The weights of these films measured by the microbalance were 20 and 18 μg, respectively. According to the XRD patterns (not shown here), the crystal structures of anodic deposited $MnO_x \cdot nH_2O$ films on the Ni and CNT/Ni substrates are amorphous. The FE–SEM images shown in Fig. 3.2 reveal the surface morphologies of the anodic deposited $MnO_x \cdot nH_2O$ films on the Ni and CNTs/Ni substrates. The surface morphologies of $MnO_x \cdot nH_2O$ film grown on the Ni substrate (Figs. 3.2 (a) and (b)) indicate that the relatively smooth surface of the film with an average particle size of 25 nm. However, the surface morphology of the MnO_x film on the CNTs/Ni substrate is quite different. As shown in Figs. 3.2 (c) and (d), it consists of the 10~25 nm MnO_x primary and secondary (i.e., agglomerates) nanoparticles on the substrate

surface. The different MnO_x morphologies between two substrates could be owing to the different initial surface morphologies between Ni and CNTs/Ni substrates. The BET measured surface area of the MnO_x/Ni is 6.0 m^2/g, and the increasing surface area based on the mass of MnO_x only is 58.9 m^2/g. However, the BET measured surface area of the MnO_x/CNTs/Ni substrate is 20.2 m^2/g, and the increasing surface area based on the mass of MnO_x only is 82.0 m^2/g. The BET surface area of MnO_x/CNTs/Ni has been found to be larger than that of MnO_x/Ni due to the application of CNTs. Obviously, the MnO_x nanoparticles grown on the CNTs/Ni substrate have larger surface area than that on the Ni substrate. Such a porous MnO_x film might provide a large redox reaction area to achieve fast charge/discharge rates.

In order to realize the influence of charge/discharge cycling on the morphologies of MnO_x on the substrate, the morphologies of MnO_x/Ni and MnO_x/CNTs/Ni films after 100 cycles CV measurements are observed and shown in Fig. 3.3. It indicates in Figs. 3.3 (a) and (b) that some of the amorphous MnO_x particles reveal its particle size of 45 nm on the Ni substrate, and others merge to larger secondary particles and the smoother surface formed (region A). The surface morphology of MnO_x/CNTs/Ni is shown in Figs. 3.3 (c) and (d) after 100 cycles CV measurement. Few MnO_x nanoparticles tend to detach from the surface, as the average diameter of MnO_x nanoparticles increases to 30 nm with an increase in the cycles of CV measurement, while no MnO_x particles would merge into the larger ones like region A. After such a CV cycling, the BET surface area of the MnO_x/Ni electrode changes to 3.36 m^2/g, and that of the MnO_x/CNTs/Ni electrode 19.83 m^2/g. It is quite obvious that the reaction area of MnO_x/Ni electrode has larger reduction due to the change of surface morphologies. Therefore, the MnO_x/CNTs/Ni electrode would show the better reversibility since it has a–MnO_x nanoparticles grown on the CNTs/Ni substrate that could keep the smaller particles from merging into the larger ones after the CV cycles.

Figure 3.4 illustrates the TEM images of the CNT and anodic deposited MnO_x. It is indicated in Fig. 3.4(a) that the CNTs are all multiwall with an average diameter of 20 nm. The MnO_x particles on the CNTs/Ni have the diameters ranging from 10 to 25 nm (Fig. 3.4(b)). The SAED pattern (inset in Fig. 3.4(b)) of the MnO_x nanoparticle could not be indexed to any of the MnO_x lattice structures as these particles are all amorphous. The EDX spectrum, as shown in Fig. 3.4(c), of MnO_x nanoparticles determined by the EDX spectrometer attached to the TEM, reveals that manganese (Mn) and oxygen (O) are the main constituents of the nanoparticles while the Cu peak generated by the Cu grid. It also shows that the chemical composition is nonstoichiometric manganese oxide, $MnO_{1.70}$, anodic deposited on the substrates.

3.2 Electrochemical characterizations of MnO_x/CNTs composite electrodes

Figure 3.5(a) shows the CV curves of the MnO_x/Ni and MnO_x/CNTs/Ni composite electrodes in 0.1 M Na_2SO_4 solution at 25 ^oC cycled under a potential in the range from 0 to 1.0 V with a scan rate of 5 mV/s. Both the CV curves are almost rectangular in shape, which implies that both of them exhibit capacitive behavior. The mean specific capacitances of MnO_x/Ni and MnO_x/CNTs/Ni composite electrodes based on the mass of MnO_x (Fig. 3.5(a)) are 233 and 415 F/g, respectively. The CCD curves of MnO_x/Ni and MnO_x/CNTs/Ni composite electrodes indicated in Fig. 3.5(b) depict that the slopes for both curves are not constant. The average specific capacitances of MnO_x/Ni and MnO_x/CNTs/Ni electrodes calculated from the average slope based on the Eq. 2.1 are 241 and 418 F/g, respectively. The larger specific capacitance existed in MnO_x/CNTs/Ni electrode may be attributed to that the porous surface of this electrode would provide a larger surface area between the aqueous

electrolyte and the MnO_x nanoparticles to facilitate redox reaction. This suggestion could be demonstrated by the CV measurements with various scan rates. Effect of scan rate on the CV curves of the MnO_x/CNTs/Ni electrode is shown in Fig. 3.6(a). All of the curves were almost rectangular and show a capacitive behavior. The mean specific capacitances of MnO_x/CNTs/Ni with the scan rate of 10, 20, 40 and 100 mV/s are 410, 407, 403 and 386 F/g, respectively. These CV curves demonstrate that the anodic deposited MnO_x/CNTs/Ni composite electrode has excellent redox reversibility. Figure 3.6(b) shows the influence of potential scan rate on the capacitance recorded with scan rate from 5 to 100 mV/s for MnO_x/Ni and MnO_x/CNTs/Ni composite electrodes. The specific capacitances at the scan rate of 5 mV/s calculated from the CV curves of these two electrodes are the highest, which are 233 (MnO_x/Ni) and 415 (MnO_x/CNTs/Ni) F/g. As shown in the figure, the specific capacitances of these electrodes decrease as the potential scan rate increases. As the potential scan rate is raised to 100 mV/s, the specific capacitance of MnO_x/Ni electrode decreases to 126 F/g which is 54 % of that measured with a scan rate of 5 mV/s, while the specific capacitance of MnO_x/CNTs/Ni is 386 F/g which is 93 % of that measured with a scan rate of 5 mV/s. The MnO_x/CNTs/Ni electrode exhibits good reaction reversibility and less capacitance decay for faster potential scan rate, probably due to the high conductivity of CNTs that acts a good current collector with a low contact resistance. In addition, the better dispersion of MnO_x nanoparticles over the CNTs/Ni substrate also provide a large activated surface area to redox reaction, and consequently keep 93 % capacitance at the scan rate of 100 mV/s. The capacitive ability and reaction reversibility of MnO_x/CNTs composite electrode in the present study are better than those of other groups' reports on MnO_x electrode[183,184].

The electrochemical characteristics of the electrode can be realized from the electrochemical impedance spectrum (EIS) and the corresponding equivalent circuit

model. The ac impedance responses of MnO_x/Ni and MnO_x/CNTs/Ni electrodes measured at the open–circuit potential (OPC ~ 300 mV *vs.* SCE) in the 0.1 M Na_2SO_4 are shown in Fig. 3.7, indicating that both of these two spectra are composed of an arc in the high frequency region and a line in the low frequency region. This phenomenon in the high frequency region could be caused by the double layer process as the response of this process is faster than that of faradaic process. In the high frequency region, the intercepts with real impedance (Re (Z)) axis of MnO_x/Ni and MnO_x/CNTs/Ni are 0.863 and 0.347 Ωcm^2, respectively. This value is considered as the total electrical resistances of electrode material (R_m), the electrolyte (R_e), and the electrical leads (R_l). As the R_e and R_l are almost the same through the experiments, the decrease of total resistance could have contributed to the low resistance of electrode materials. The electrode resistance is composed of the resistance of the electrode material and the contact resistance between materials. It could be suggested that the CNTs/Ni electrode which provides a rough surface and large contact area between electrode and MnO_x. Therefore, the total resistance of MnO_x/CNTs/Ni becomes smaller than that of MnO_x/Ni. The imaginary part of impedance plot of MnO_x/CNTs/Ni electrode in the high frequency region was larger than that of MnO_x/Ni electrode, which is attributed to the double layer capacitor, formed by the high surface area and well dispersed MnO_x nanoparticles on CNTs/Ni substrate. However, in the low frequency region, the faradaic reaction was the main effect as shown in approximately linear increase in the imaginary part of the impedance spectra. The slope of impedance plot of MnO_x/CNTs/Ni electrode is larger than that of MnO_x/Ni electrode as the faradaic capacitor is formed by the highly electroactive material of MnO_x deposited on the CNTs/Ni substrate. Therefore, the large surface area of MnO_x/CNTs/Ni electrode with a high electrochemical activity exhibits better capacitance behavior.

The electrochemical stability of electrode was investigated by applying cyclic CV measurements. Figure 3.8 shows the plots of the specific capacitance of MnO_x/Ni and MnO_x/CNTs/Ni electrodes *vs.* cycle of CV test. The specific capacitances of MnO_x/Ni fall to 83 % and 70% of the original value after 100 and 600 cycles of CV test, respectively. The specific capacitance drops quickly to 11 % of the original value after 1000 cycle tests. But those of MnO_x/CNTs/Ni electrode have less reduction, the capacitances are 97% and 91 % after 100 and 600 cycles tests, respectively. The capacitance of MnO_x/CNTs/Ni remains 79 % of the original value until 1000 cycles CV test. The cyclic voltammetry tests indicate that the a–MnO_x/CNTs/Ni composite electrode shows the good electrochemical characteristics.

3.3 Conclusions

The a–MnO_x/CNTs/Ni composite electrodes synthesized by anodic deposition at 25 ^oC in a 0.16 M $MnSO_4 \cdot 5H_2O$ solution revealed 10~25 nm amorphous MnO_x nanoparticles on the CNTs/Ni substrate. Such nanocomposite electrodes have shown much better energy storage capabilities than those deposited on the Ni substrate mainly due to low resistance and large surface area of the nanocomposite electrodes. The specific capacitances of MnO_x/CNT/Ni electrodes were 415 and 418 F/g as obtain from CV measurement with a scan rate of 5 mV/s and calculated from CCD test, respectively. Furthermore, the a–MnO_x/CNTs/Ni nanocomposite electrode preserved 79 % of its original capacitance in the 1000 cycles of operation. Such nanocomposite electrodes exhibit good capacitance properties and excellent reversibility. Therefore, the a–MnO_x/CNTs/Ni nanocomposite electrode may be appropriate for supercapacitor applications.

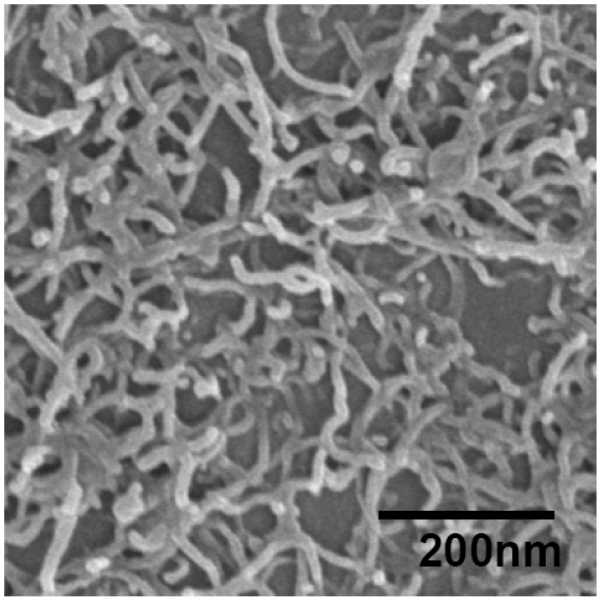

Figure 3.1 SEM photograph of CNT/Ni surface.

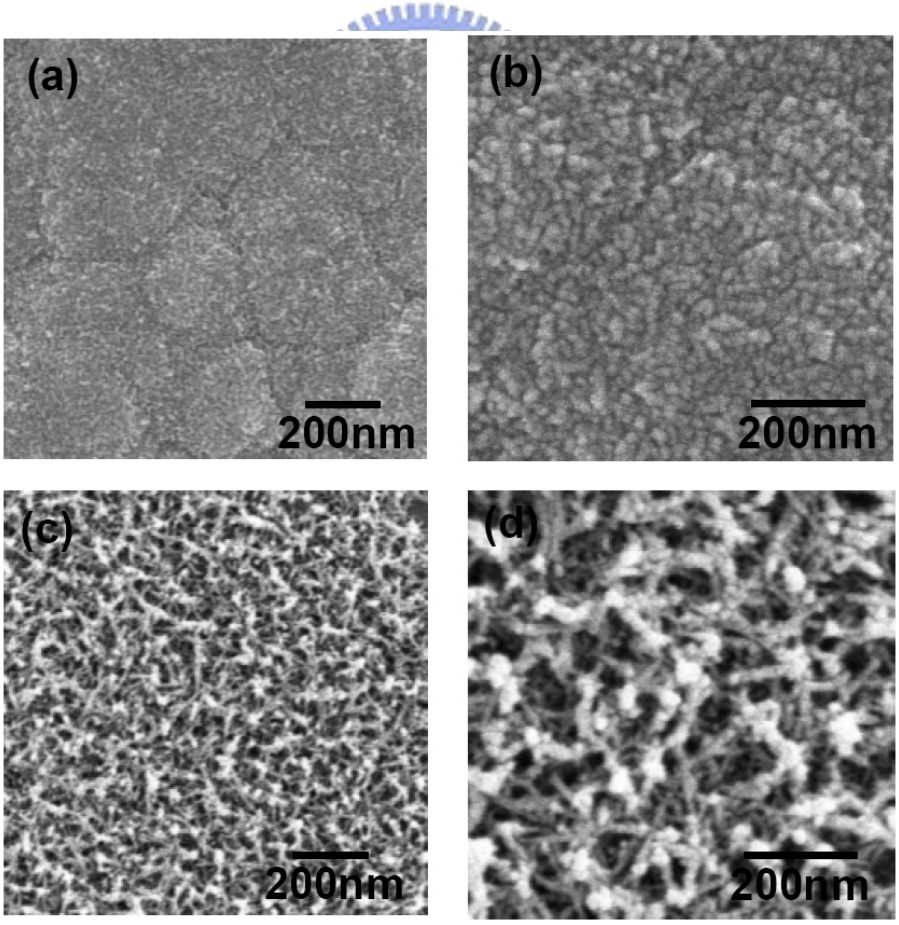

Figure 3.2 SEM photographs of (a, b) MnO_x/Ni surface and (c, d) MnO_x/CNT/Ni surface.

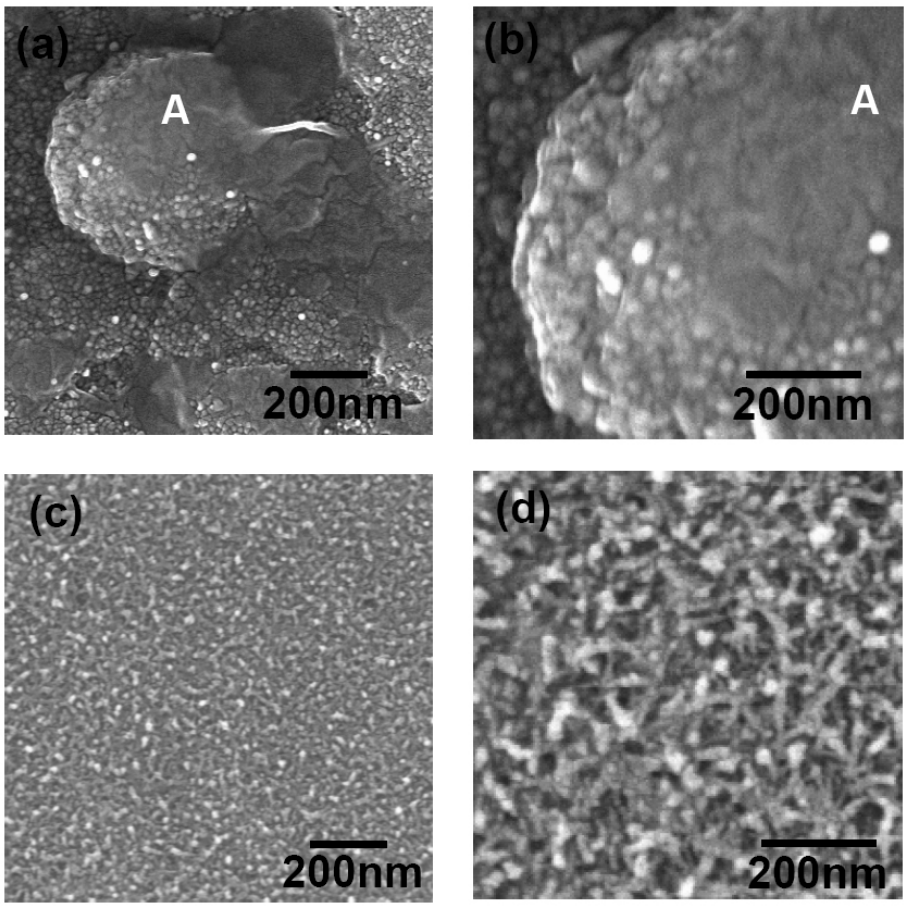

Figure 3.3 SEM photographs of (a, b) MnO_x/Ni surface and (c, d) MnO_x/CNT/Ni surface after 100 cyclic voltammetry test.

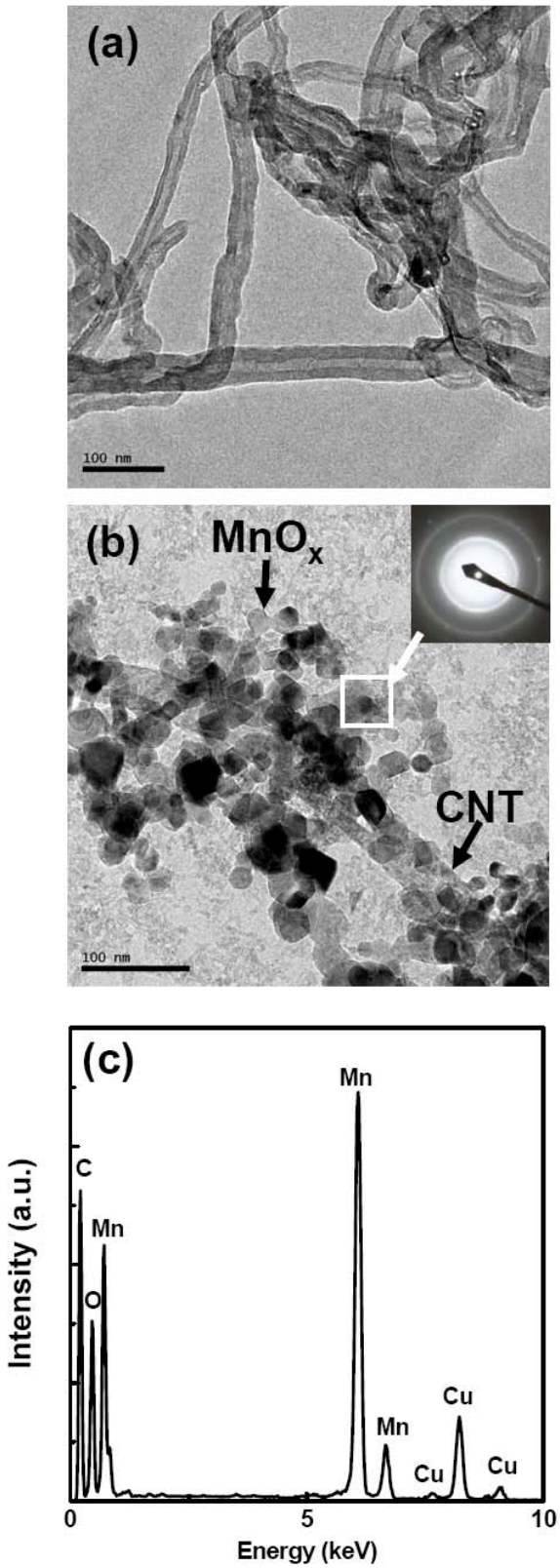

Figure 3.4 (a) TEM image of CNT, (b) TEM image of MnO_x/CNT nanocomposite and the inset is the SEAD of MnO_x nanoparticles and (c) EDX spectrum of MnO_x nanoparticles.

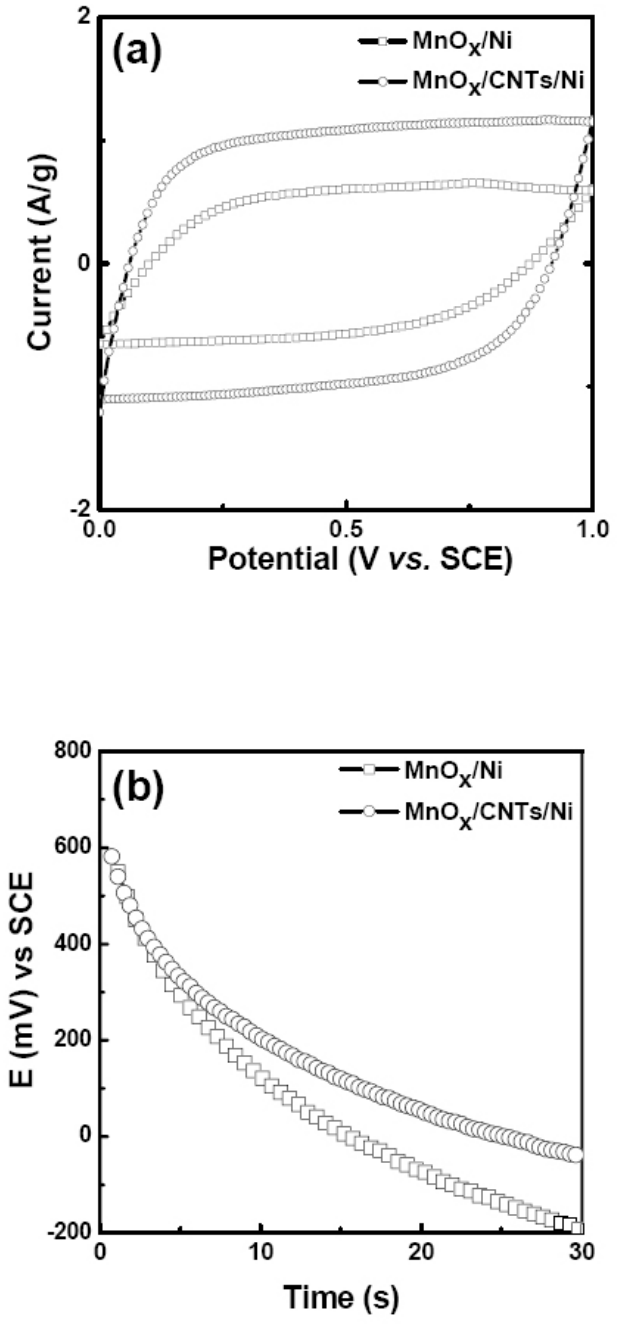

Figure 3.5 (a) CV curves for the a–MnO_x/Ni and a–MnO_x/CNTs/Ni electrodes in 0.1 M Na_2SO_4 solution at 25 ^oC with a potential scan rate of 10 mV/s. (b) CCD curves for the a–MnO_x/Ni and a–MnO_x/CNTs/Ni electrodes.

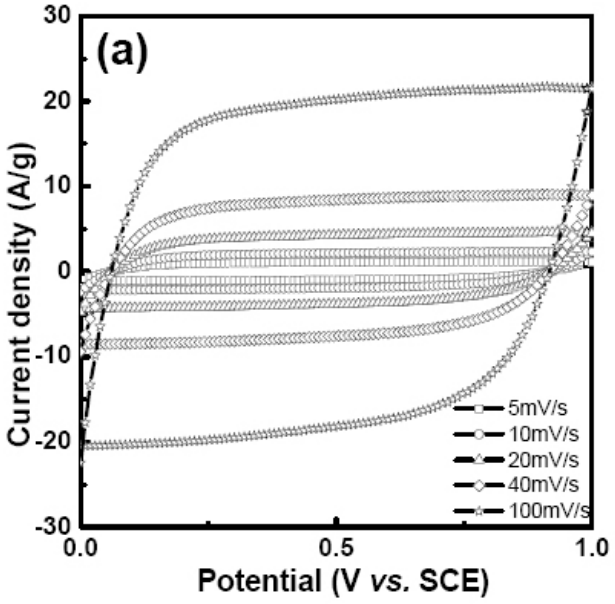

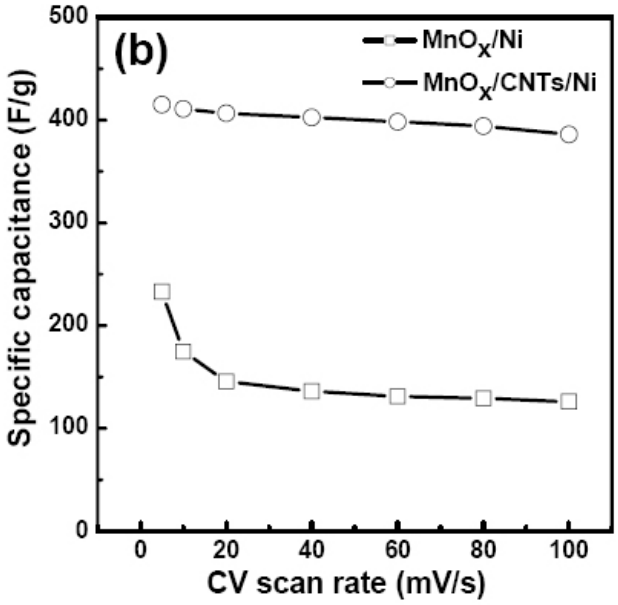

Figure 3.6 (a) Variation of CV curves of the a–MnO_x/CNTs/Ni electrode with potential scan rates of indicated. (b) Variation of specific capacitances of a–MnO_x/Ni and a–MnO_x/CNTs/Ni electrodes with CV scan rate.

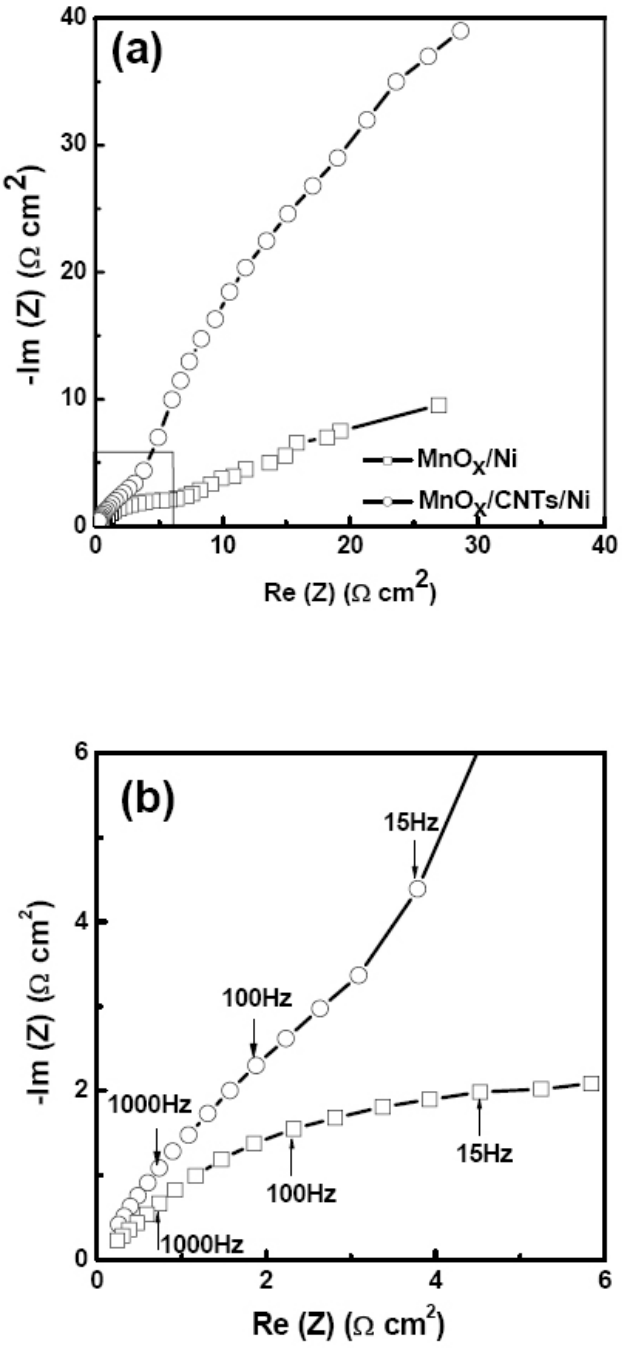

Figure 3.7 (a) A Nyquist impedance spectra of a–MnO_x/Ni and a–MnO_x/CNTs/Ni electrodes measured at the OCP (10 mV vs. SCE). (b) The impedance spectra in the high frequency region.

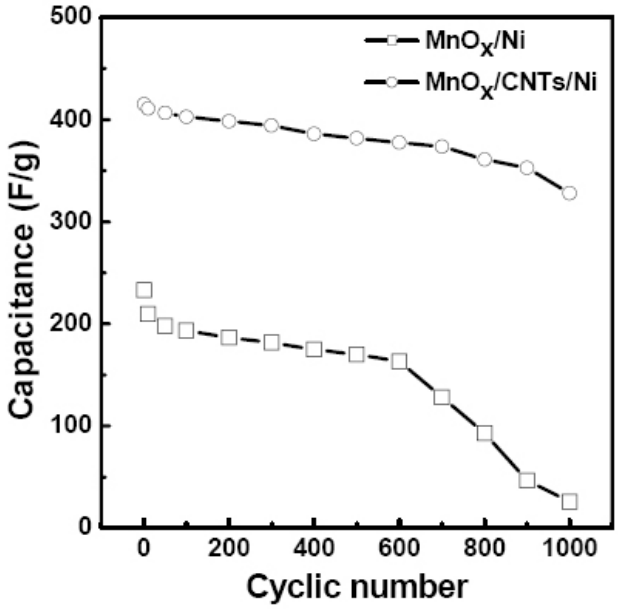

Figure 3.8 Stability tests of the a–MnO_x/Ni and a–MnO_x/CNTs/Ni electrodes. CV tests were measured at 10 mV/s in 0.1 M Na_2SO_4 solution.